A&A 384, 303–316 (2002)
DOI: 10.1051/0004-6361:20011819

Astronomy & Astrophysics

An erupting macrospicule

Characteristics derived from SOHO-CDS spectroscopic observations

S. Parenti, B. J. I. Bromage, and G. E. Bromage

Centre for Astrophysics, University of Central Lancashire, Preston PR1 2HE, UK

Received 9 November 2001 / Accepted 20 December 2001

Abstract. We report results from the analysis of a sequence of SOHO/CDS observations obtained off-limb in the south polar coronal hole on 6 March 1998. Three successive data sets were obtained with the Normal Incidence Spectrometer (NIS), the first of which showed a jet-like feature visible in the chromospheric and low transition region lines. The morphological characteristics of this feature suggested it was a macrospicule. The two remaining observations of the same region indicated a quiet coronal hole with a density of 10^8 cm^{-3} and a temperature rising from 0.95×10^6 K near the limb to 1.2×10^6 K at about 4.7×10^4 km above the limb. These data were averaged and used as "background" for the macrospicule observation. The resulting subtracted spectra showed more details of the feature. In particular, a cloud of plasma was detected at about 3×10^4 km above the limb. The macrospicule was found to have a density of the order of 10^{10} cm^{-3} and a temperature of about $2{-}3 \times 10^5$ K. The initial outflow velocity near the limb was over 80 km s^{-1}. This decreased to a terminal value of 26 km s^{-1} above about 6×10^4 km.

Key words. Sun: corona – Sun: activity

1. Introduction

The first observation of EUV macrospicules was made by Bohlin et al. (1975) who attributed this name to jet-like features of coronal holes which appeared similar to, although larger than, Hα spicules.

EUV macrospicules appear as columns of chromospheric material extending from the limb into the corona. Their widths range between 5″ and 15″ and they are from 5″ to 60″ in length, with a lifetime of a few minutes to about 40 min (Dere et al. 1989; Bohlin et al. 1975). The brightest images of these features in the corona are given by the He I ($\log T = 4.5$), He II ($\log T = 4.9$) and O V ($\log T = 5.4$) lines. Bohlin et al. (1975) found no evidence of emission above $3{\times}10^5$ K. However, more recently Pike & Harrison (1997) have observed macrospicule emission in a Mg IX line, emitted at around 1 MK.

Karovska & Habbal (1994) studied the evolution of C III ($T = 7.4 \times 10^4$ K) macrospicules using the Harvard/S-O55 spectroheliometer on Skylab. With its 5″ telescope resolution, they were able to resolve the small-scale morphology of these structures and study their evolution. The macrospicules often showed an arch-like base, that extended into the corona as a column-like structure. These structures were also characterized by ejection of material followed by the disappearance of the macrospicule, on a time-scale of a few minutes. This study suggested that macrospicules are dynamic events that evolve rapidly. Habbal & Gonzalez (1991) observed some macrospicules at radio frequencies of 4.8 GHz. These had the same dimensions as the EUV macrospicules. Moreover, they found that these structures were composed of a cool core ($4{-}8 \times 10^4$ K) surrounded by a hotter sheath ($1{-}2 \times 10^5$ K) that released plasma from the upper part of the structure. This multithermal structure was later observed in the EUV waveband by Pike & Harrison (1997).

Velocity studies of macrospicules have revealed red and blue Doppler shifts on opposite sides of the feature's central axis (Pike & Mason 1998; Pike & Harrison 1997; Banerjee et al. 2000). The apparent velocities increase with solar distance and reach a maximum value of 60 km s^{-1} between 20 and 30 arcsec above the macrospicule footpoints. Pike & Mason (1998) referred to this apparently rotating plasma as a *solar tornado*.

Macrospicules have also been identified as Hα features (e.g. Cook et al. 1984). Studies addressing the relationship between Hα and EUV macrospicules have produced conflicting results. Wang (1998) found that each of the He II (304 Å) macrospicules they observed had a Hα counterpart, while Moore et al. (1977) had earlier found that this was not always the case. In the light of this, Georgakilas et al. (1999) suggested that there might be two subclasses of He II macrospicules: polar surges and giant spicules.

Send offprint requests to: S. Parenti,
e-mail: sparenti@uclan.ac.uk

The former appear as complex structures, with strong velocity gradients. The latter are jet-like features.

In this work we investigate a feature which has the morphology of a macrospicule, seen above the limb in the south polar coronal hole. The data available gave us the rare opportunity to obtain a *background* to be subtracted from the image containing the macrospicule. In this way, the characteristics of this feature could be studied and compared with those of the surrounding coronal plasma.

2. The observations

On 6 March 1998, three successive off-limb observations were made of a region of the south polar coronal hole. The full spectra (from 308 to 381 Å and from 513 to 633 Å) of a $120'' \times 120''$ raster were obtained by the Normal Incidence Spectrometer of CDS on SOHO (Harrison et al. 1995). A raster was built up by scanning the slit from west to east in 30 steps, each with an exposure time of 160 s. The three rasters obtained were all centred at a distance of 1.08 $R_\odot$ ($1050''$) from Sun centre at a longitude of $-0.1°$ ($-2''$) as shown in Fig. 1. The spatial pixel size was about $3.4''$ in Y-direction and about $4''$ in the X-direction.

The standard CDS software was used for initial processing of the data (de-biasing, then flat-field correction and cosmic ray removal). The spectra were then fitted using multiple Gaussian line-fitting (Haugan 1997), and the intensity calibration from Del Zanna et al. (2001) was applied.

This differs a little for some of the lines used here, compared with the standard calibration. However, the analysis employed involves only line-ratio diagnostics and the discussion of the results focuses on variations in the derived densities and temperatures rather than absolute values. Hence the conclusions are not dependent on which calibration was used.

The first raster was obtained between 10:41 and 12:57 UT. Monochromatic images of the observed region at this time are given in Fig. 2. In this observation a spike-like feature appears at the top left corner of the raster, in images from chromospheric and low transition region lines, while it is scarcely visible in images from coronal lines (the Mg X shown in the figure has a contribution from an O IV line; see discussion in Sect. 7). The solar limb is towards the top, just out of the field of view, at solar $Y = -974''$, i.e. about $19''$ from the top of the image.

It is important to note that each raster contains both spatial and temporal information. As already stated, each raster is made up of a sequence of 30 exposures, obtained by moving the slit from west to east. Each exposure lasts 160 s and an interval of about 270 s passes between the start of successive exposures. The solar rotation can be neglected, so two successive positions of the slit give the plasma intensity observed in different locations ($4''$ apart) with a time delay of about 270 s.

Referring to the raster images, each column represents the image of the slit obtained during one exposure.

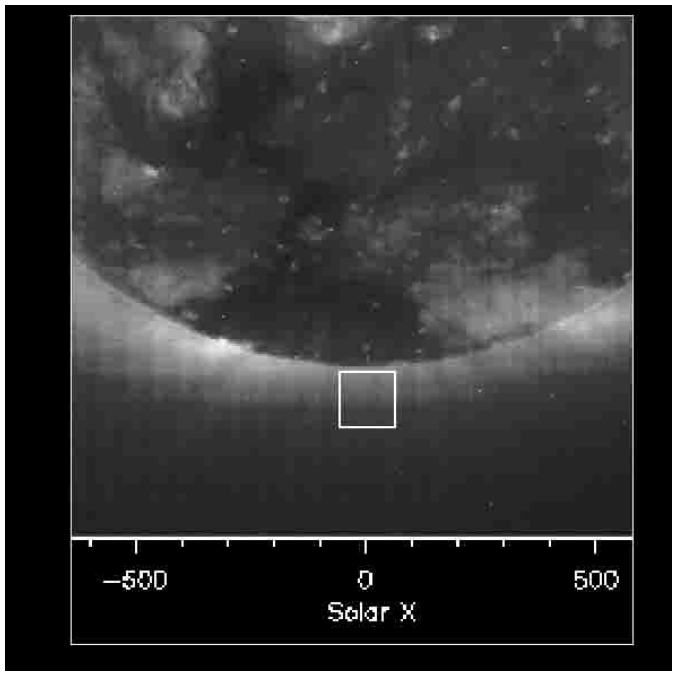

Fig. 1. Detail of 195 Å SOHO/EIT image of the solar corona taken 6 March 1998. The CDS raster is superimposed as a white rectangle to show its field of view. The image shows a well defined coronal hole occupying the south pole.

Numbering the columns from left to right, starting from 0, the feature is seen to be bright over several pixels along the Y-direction in Cols. 4–6 (corresponding to solar $X \sim -40''$). The O V image shows the feature extending about $70''$ from the limb with a width of $\approx 12''$. This morphology and temperature of emission are characteristic of a macrospicule.

The other two successive observations of the same area at 12:57–15:13 UT and 15:13–17:29 UT, do not show any indication of the feature. Considering that the time between two successive rasters is about two hours, the feature appears to be short-lived, also a characteristic of macrospicules. Moreover, the evolution of the feature in successive columns indicates a time scale of the order of 20 min (see below).

3. The background

The other two rasters show the coronal hole without any feature apparent at the location of the macrospicule. These two sets of observations were therefore averaged to provide a *background* to be subtracted from the first raster. The background data were studied for evidence of plume plasma in the line of sight to the macrospicule. If a plume were present it might vary during the observations, which would affect the analysis of the macrospicule plasma after the background subtraction. A plume emits mainly at upper transition region temperatures, similar to the temperatures at which the macrospicule is seen here, and could therefore possibly cause confusion. Averaging over the two observations does not degrade information about

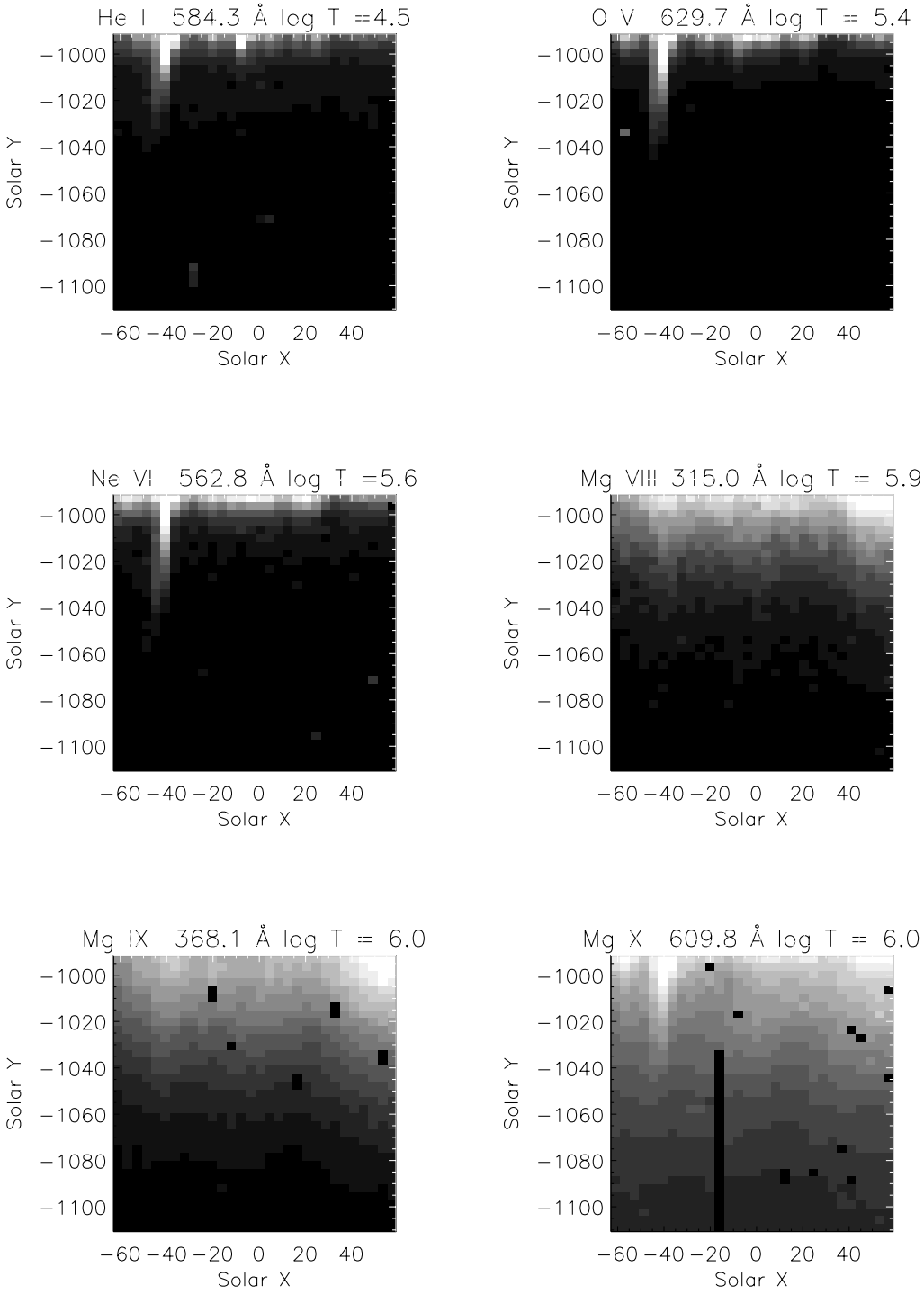

Fig. 2. Monochromatic images of the first raster in selected spectral lines. The south solar limb is about 20″ above the top margin of the image. The macrospicule feature is brightest at Cols. 4–6, counted from 0 as the easternmost column of the image. It is clearly visible in the chromospheric and transition region lines and faintly visible in the lower coronal emission (Mg X 609.793 Å is blended with O IV 609.827 Å). Note that the *time* sequence of observations started from the west (r.h.s.) of the images, e.g. Col. 6 was exposed before 5.

the presence of plume plasma. The life-time of a plume is of the order of days (Deforest et al. 1997), while in our case only information on a time scale of hours could be lost by averaging. Once the average was formed, the two rows of pixels closest to the limb (from −60″ to 25″ along the east-west direction) were selected, and the average of the spectra over the two rows was obtained. A multi-Gaussian fit to the spectra was performed. The fitting procedure is time-consuming, so the analysis was limited to the area of interest, excluding data furthest from the macrospicule. Profiles of intensity along the X-direction were thus obtained (Fig. 3).

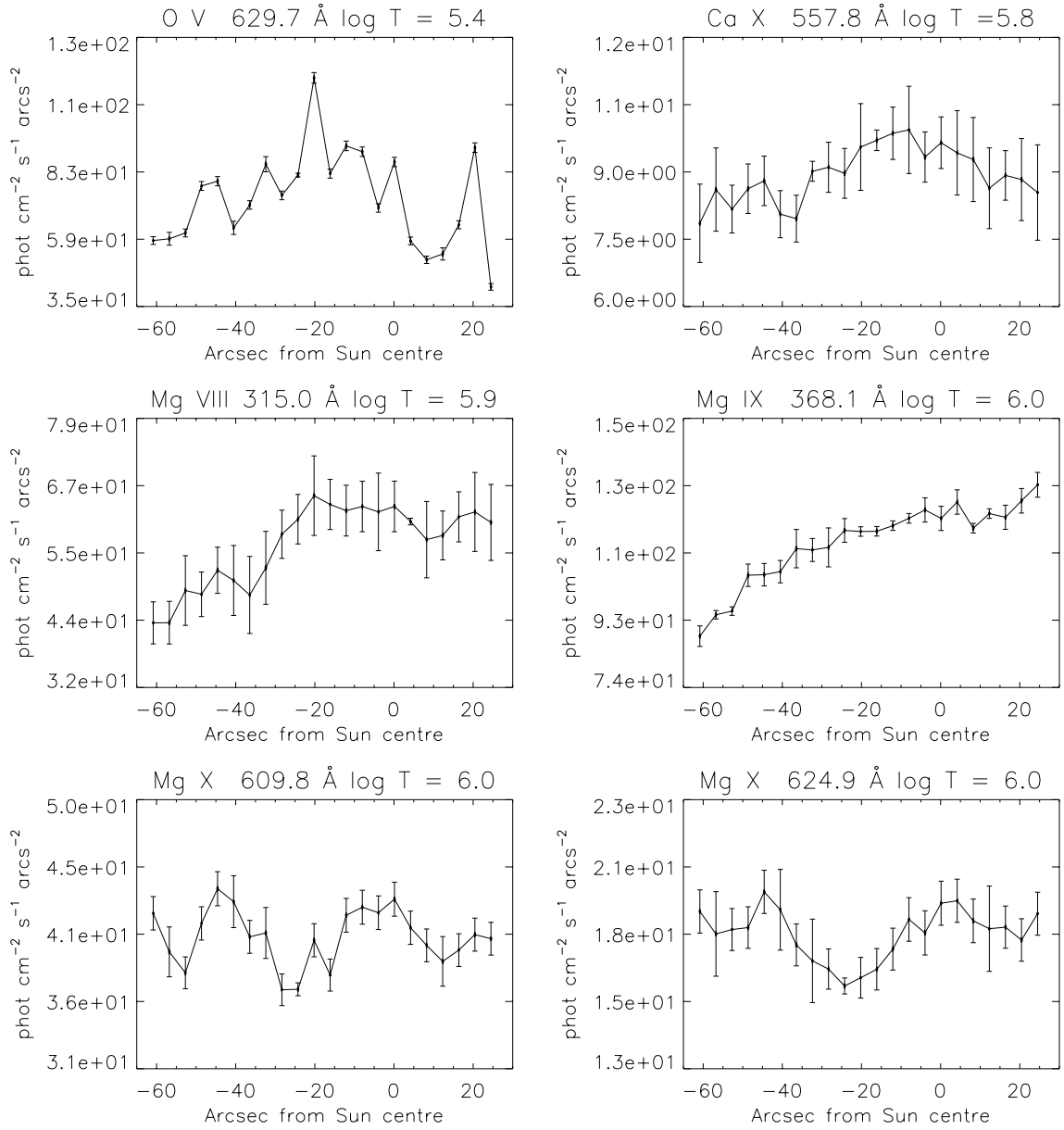

Fig. 3. Profiles along the X direction of integrated intensities at a distance of about $-1000''$, south of Sun centre, for ions emitting at different temperatures. The data are from the observations used as "background".

An intensity profile across plume and interplume regions generally shows an enhancement at the plume location, visible in the chromospheric and transition region lines (Young et al. 1999; Del Zanna 1999). In Fig. 3, the only lines to show a clear trend in intensity along the X-direction are the Mg VIII and Mg IX lines. They increase towards the west. Looking at the full raster monochromatic images of Fig. 2, a bright feature can be seen in the top right hand corner at those wavelengths (the same feature is visible in the background data). The temperature of this enhanced emission indicates the presence of plume material westward of about $-30''$ (see Fig. 5, below). The macrospicule lies outside this region at about $-40''$.

The line ratio technique (Mason et al. 1997) was applied to obtain electron density and temperature, using the CHIANTI database (Landi et al. 1999) and the Mazzotta et al. (1998) ionization equilibrium. The profile of density along the solar-X direction shown in Fig. 4 was obtained from the Si IX 349.87/345.13 Å ratio. Using the same line ratio Young et al. (1999) found a difference greater than a factor of two between the density in the plume at its base and that in the interplume region. Del Zanna & Bromage (1999), analysing a plume at the coronal hole limb, found very little difference in density between the plume and interplume regions at this temperature. Wilhelm et al. (1998b), using the Si VIII 1440/1445 Å ratio, found a factor 2 difference in density between the centre of the plume and the interplume region, over approximately the same solar distance as the data used here. Figure 4 shows a small increase in density from east to west, along the X-direction, but there

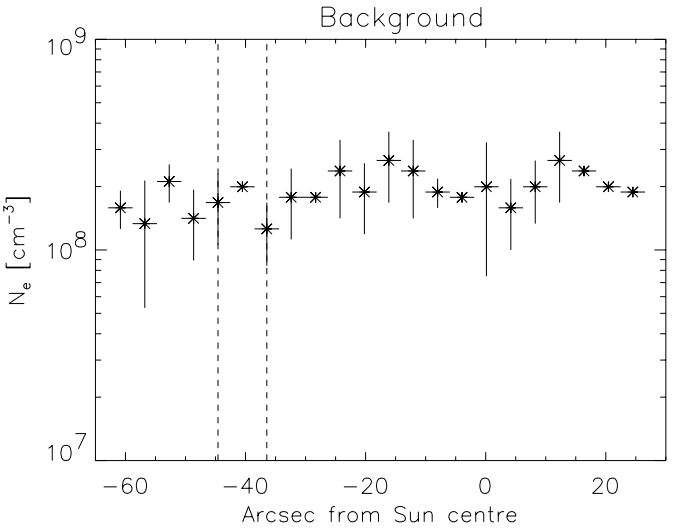

Fig. 4. Electron density (N_e) along the solar X direction for the background coronal hole, derived from the ratio Si IX 349.9/345.1. The vertical dashed lines indicate the region occupied by the macrospicule. East is to the left.

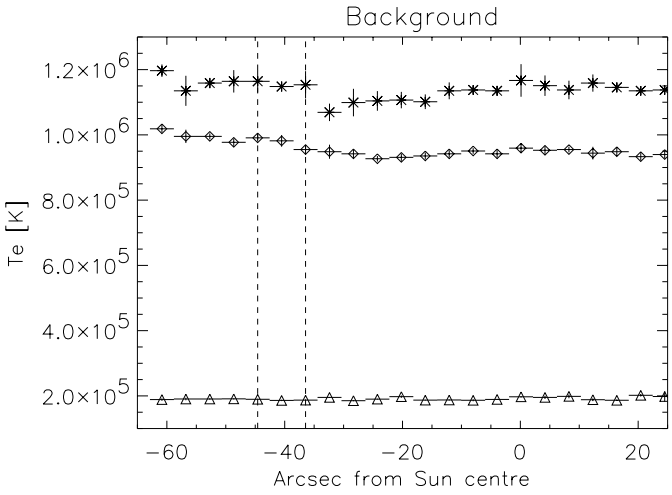

Fig. 5. Electron temperature (T_e) along the solar X direction for the background coronal hole. Asterisks represent the temperature from the Fe XII 364.467/Fe X 345.723; diamonds from Mg X 624.9/Mg IX 368; triangles from O V 629.730/O IV 554.513. The vertical dashed lines indicate the region occupied by the macrospicule. East is to the left.

is no significant distinction between plume and interplume regions.

Figure 5 shows the profile of temperature derived from the Fe XII 364.467/Fe X 345.723, Mg X 624.9/Mg IX 368 and O V 629.730/O IV 554.513 ratios. The ratios are sensitive to different components of the multi-thermal plasma observed along the line of sight. While the temperature from the oxygen ratio remains almost constant, the temperatures obtained from the iron and magnesium ratios show a small decrease from east to west. Wilhelm et al. (1998b) found a variation of about 20% in temperature between plume and interplume regions, with the plume being slightly cooler. Del Zanna & Bromage (1999) also found plumes to be cooler than the surrounding coronal hole, with emission predominantly over a narrow temperature range just below 10^6 K. The Mg X/Mg IX ratio, which is sensitive to this range, clearly indicates a temperature characteristic of plume material in the west of the region, while the macrospicule is to the east, in an area at a slightly higher temperature, characteristic of interplume/coronal hole plasma.

In conclusion, the spectra obtained by averaging the 2nd and 3rd data sets show signatures of plume material but not in the area occupied by the macrospicule. Hence this average can be used as background for the macrospicule observation.

4. Macrospicule evolution

The macrospicule occupies only about three columns in the raster. This is not a sufficiently high spatial resolution to resolve the morphology of the feature along the X-direction. The observation is further affected by the length of time (272 s) between consecutive exposures (columns of the raster). It is more likely that these data show, in the variation from one column to the next, the *temporal* evolution of the macrospicule. Therefore the spatial variation between adjacent columns is ignored in this analysis.

Figure 6 shows the intensity variation of O V 629.7 Å along the Y-direction, for each of 4 exposures along the X-direction where the feature is visible. In this figure both the original data (left hand side) and the data with the "background" data subtracted (right hand side) are shown. Note that the time sequence is from top to bottom. Column 5 is the most intense, while Col. 4 shows a shoulder around $-1010''$. This behaviour is much more evident after subtracting the background (right side). The error in the intensities is derived from the errors in the line-fitting.

Figure 7 shows the same sequence for the coronal line Si IX 345.1 Å. The emission from hotter plasma is less pronounced than at chromospheric temperature. After the subtraction of the background only a very weak signal remains (note the different Y-axis scales).

To estimate the off-limb extent of the feature it is necessary to estimate the size, in arcsec, of the solar radius at the time of the observation. This was done by estimating first the location of the O V limb brightening, and then using the information that the O V peaks at $4''$ above the photospheric limb (Mariska 1992). To find the O V peak intensity, the CDS synoptic data of the day were used, and 3 columns to each side of $X = 0$ were selected from the raster. Then the O V signal was averaged over the X direction for each Y position. In this way a smoothed profile along the Y direction was obtained. Averaging over 6 pixels in the X direction removes small scale fluctuation in the signal. The profile for the O V obtained here peaked at $-977.8''$, so that $973.8''$ is the derived limb radius. It then follows that $1'' \equiv 714.7 \pm 3.6$ km for these observations, assuming an uncertainty in the pointing of about $5''$.

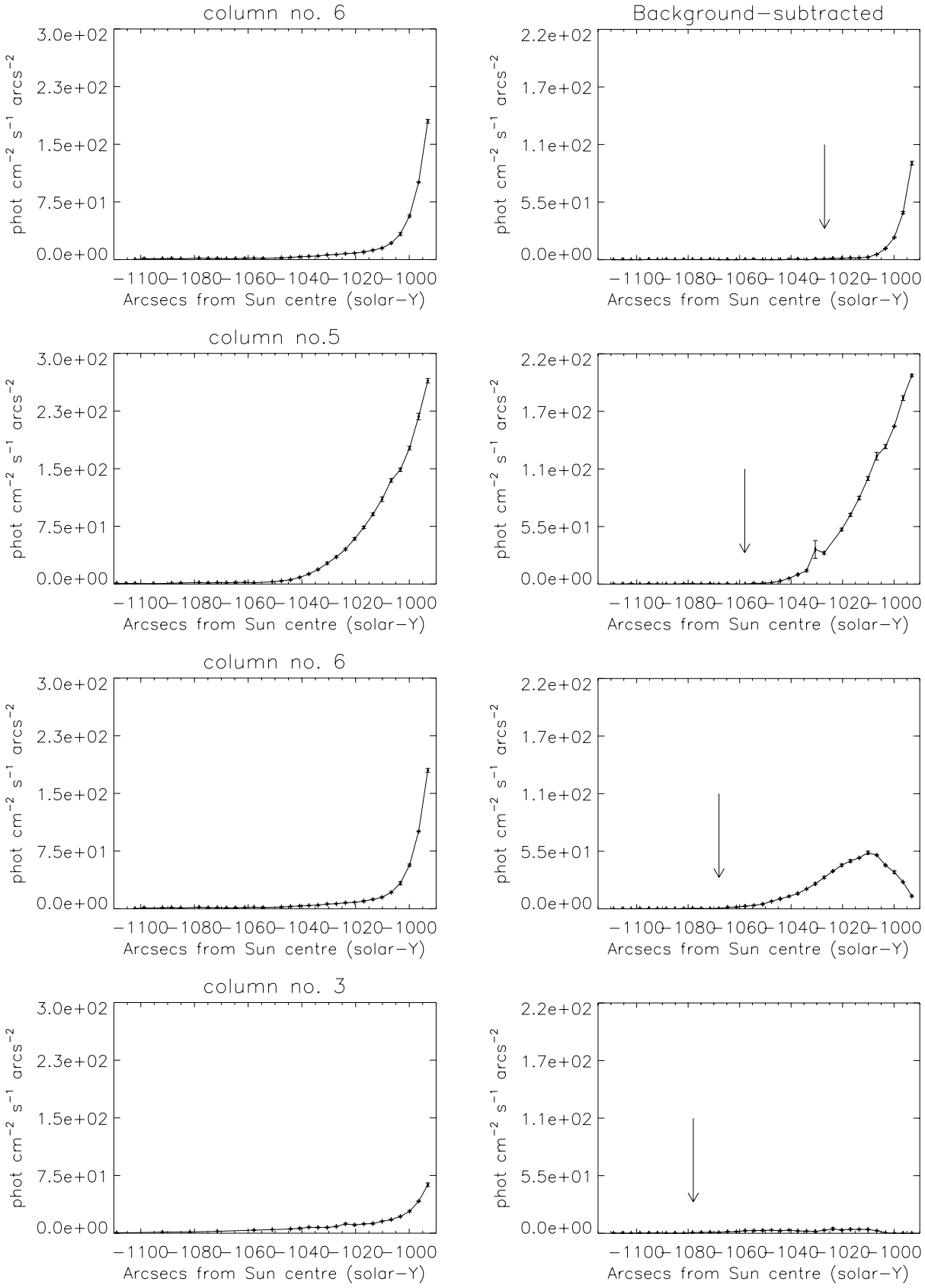

Fig. 6. Intensity profiles of the O V 629.7 Å line, along the slit (Y-direction), for each of the four Cols. 3–6, in the X-direction. On the left are the intensities from the unsubtracted observation. To the right are the intensities obtained after subtracting the background. The time between exposures (columns of the raster) is 272 s while the exposure time is 160 s. The temporal sequence is from top to bottom in this figure. The arrows indicate the position of the expansion front as described in Sect. 5 (Table 1).

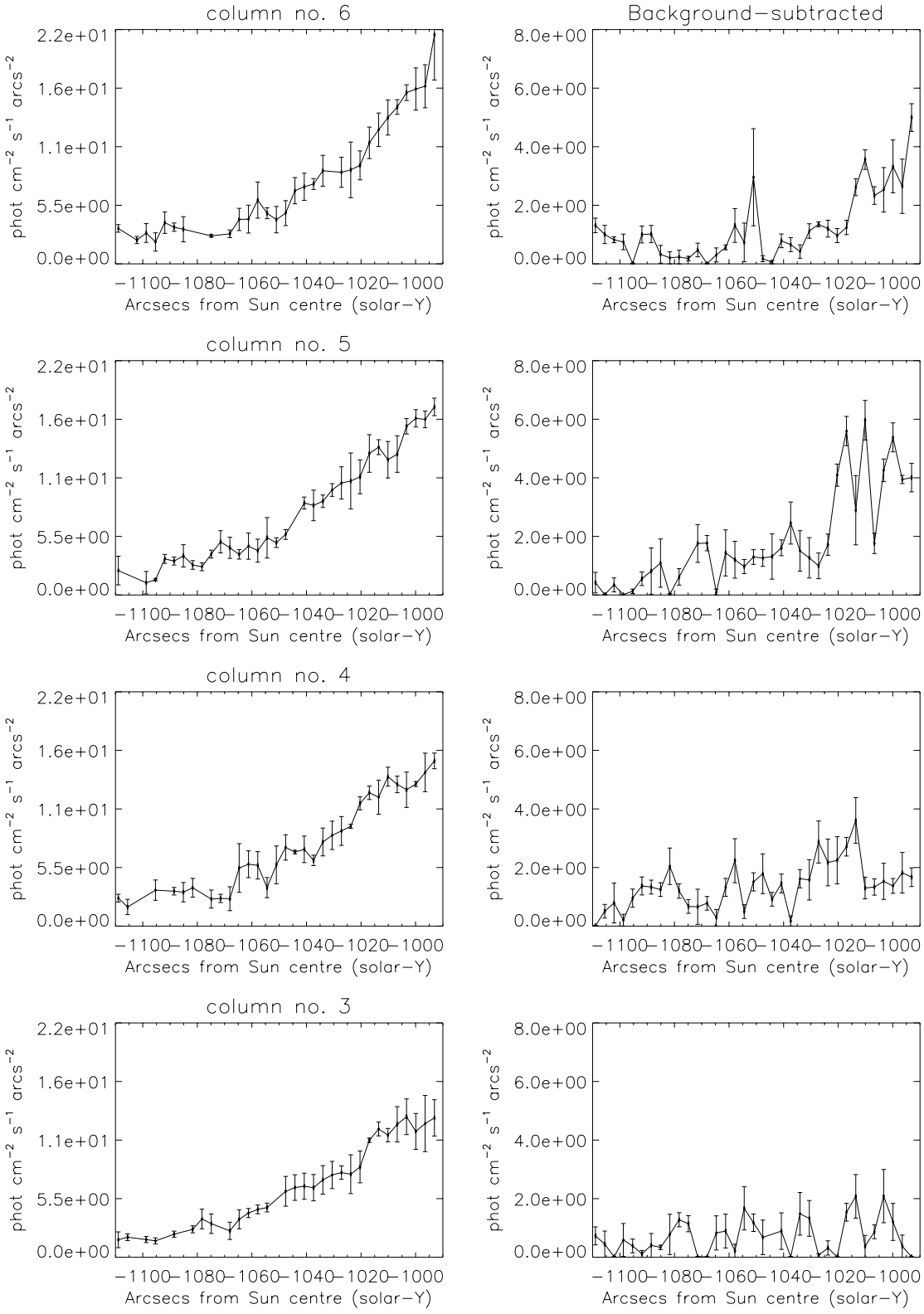

Fig. 7. Intensity profiles of the Si IX 345.1 Å line, along the slit, for each of the four Cols. 3–6, displayed in sequence from top to bottom. On the left are the intensities from the unsubtracted observation. To the right are the intensities obtained after subtracting the background. The time between exposures (columns of the raster) is 272 s while the exposure time is 160 s.

Now the macrospicule feature is $-40''$ from $X = 0$. This means that its distance from Sun centre is greater than that calculated at $X = 0$. At $X = 0$, the Y-coordinate of the closest row of pixels to the limb is $-993''$. At $X = -40''$ the distance from Sun centre is about $993.8''$, a difference that is much smaller than one

spatial pixel of the data (3.4″). Therefore this effect can be neglected.

Interpreting the sequence of plots in Fig. 6 as a temporal evolution of the feature (neglecting any spatial variation across these columns), Cols. 6 and 5 give the phase of expansion of the feature into the corona (see also Fig. 8 for a schematic view). In Col. 4 the intensity is already reducing and, looking at the right-hand figure, an isolated cloud appears with its peak of intensity at −1010″ (26 000 km from the limb). In Col. 3, just a faint brightness remains at the location of the cloud. Unfortunately, the lack of data closer to the limb limits the information available about how the macrospicule evolves nearer the Sun. In Fig. 8 a schematic picture of the macrospicule and the ejected plasmoid is shown, for each slit position. The time increases from top to bottom (as in Fig. 6) while the slit position moves from west to east. (Note that the sketch is not to scale and only the top part of the slit is indicated.)

Column 4 was selected for detailed density and temperature analysis (see Sect. 6), while the O V data displayed in Fig. 6 were used to study the flow speed of the ejected material.

5. Velocity

The radial velocity (along a radius of the Sun) of the plasma has been estimated by identifying the position of the expansion front of the macrospicule in each exposure. The first row of Table 1 gives the distance (in arcsec from sun centre) where the O V intensity drops close to zero. These values are taken from the background-subtracted data shown in Fig. 6 (indicated by an arrow in the figure). The second row shows this distance converted to km above the limb. The mid-points between successive positions are also shown. The third row of the table gives the time of each exposure relative to the start of the first (Col. 6). The fourth row gives the derived mean velocities assuming steady motion. These values were calculated assuming that 1″ on the Sun corresponded to 714.7 km (see above). The error in the velocity was estimated by assuming approximately 1 pixel error (4″) in the estimate of the distance travelled by the plasma between two successive exposures. The results clearly show a decrease in velocity with distance from the Sun. It is important to remember that the intensity in each column is integrated over the 160 s exposure time. If the maximum mean velocity of 81.6 km s^{-1} is considered, then during the exposure time the plasma would have travelled about 13 056 km (18″). This indicates that during the first exposure information about the macrospicule structure is degraded. However, the inferred deceleration (see below) soon reduces this distance so that the later exposures are only "smeared" over a distance corresponding to about 6″, less than two spatial pixels. Figure 9 (top) shows a plot of the derived velocity v. height. The lower graph shows the height of the leading edge of the cloud of plasma in the four successive exposures. The time on the X-axis starts with the

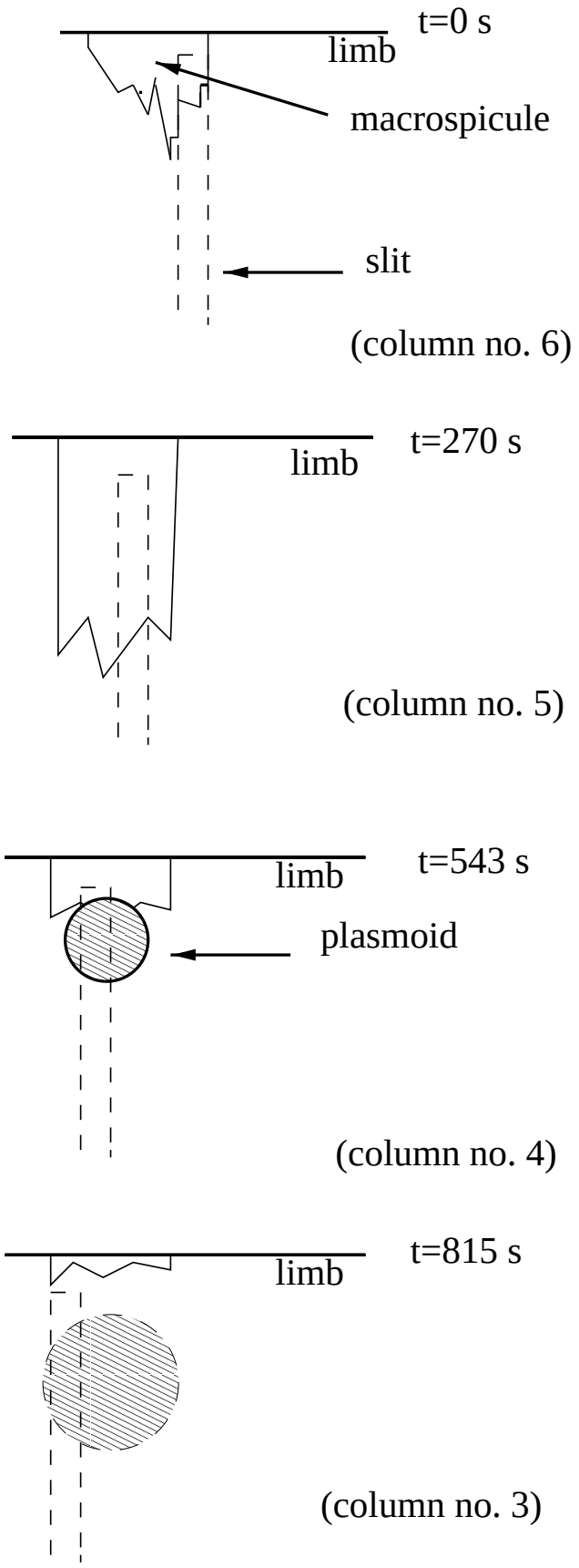

Fig. 8. Schematic picture of the macrospicule evolution during the four exposures where the macrospicule (solid line) is visible. The slit position is superimposed (dashed rectangle) at each exposure. The time increases from top to bottom, as in Fig. 6.

Table 1. Dynamics of the macrospicule plasma deduced from the O V emission.

Column	6		5		4		3
Position ± 4 (″)	−1027		−1058		−1068		−1078
(km from the limb)	38 022	49 100	60 178	63 752	67 325	70 899	74 472
Time (s)			271.6		543.2		814.8
Avg. Velocity ±10.5 (km s^{-1})		81.6		26.3		26.3	
Avg. Acceleration (km s^{-2})			−0.204		0		

beginning of the first exposure. The overplotted curve is a second order polynomial fitted to the points.

The result of this fit gives an initial velocity of 84 km s^{-1} and a (constant) deceleration of −0.102 km s^{-2}. This deceleration is much less than the gravitational deceleration of −0.274 km s^{-2} at the Sun's surface. However, the location considered here is the corona. The deceleration due to gravity at 40 000 km above the limb is −0.244 km s^{-2}, still more than double the observed value. One reason for the difference could be an inclination of the trajectory with respect to the radial direction. For this to be the case, an angle of inclination of about 78° is required. However, with this angle, evidence of line-of-sight velocity should be seen in the data. From the parameters derived from the fit to the trajectory, a velocity of about 400 km s^{-1} would, in fact, be expected along the line of sight. This corresponds to a shift of about 0.75 Å. No such large shift was seen.

The data were also examined for evidence of smaller shifts such as have been reported by Pike & Harrison (1997). Transverse (perpendicular to the radial direction) velocities were found in Cols. 4–6, with flows of up to 17 km s^{-1} directed away from the observer (along the line of sight). No indication of rotational velocity was seen.

An alternative interpretation of the dynamics can be made by looking at Fig. 9. It is clear that the deceleration is not in fact constant as the plasmoid moves out from the limb. The last row of Table 1 shows the average deceleration derived from the average velocities. At the beginning of the plasmoid motion, the deceleration assumes a value close to that due to gravity. Later, the velocity seems to tend towards a constant value of 26 km s^{-1} (±10 km s^{-1}). With the assumption that the solar gravitation is the only force acting on the plasma, and an initial outflow velocity of 81.6 km s^{-1}, a velocity of 26.3 km s^{-1} would be reached at about 60 000 km above the limb. This is consistent with the observed flow.

The data have also been checked for evidence of O V line broadening, but none was found.

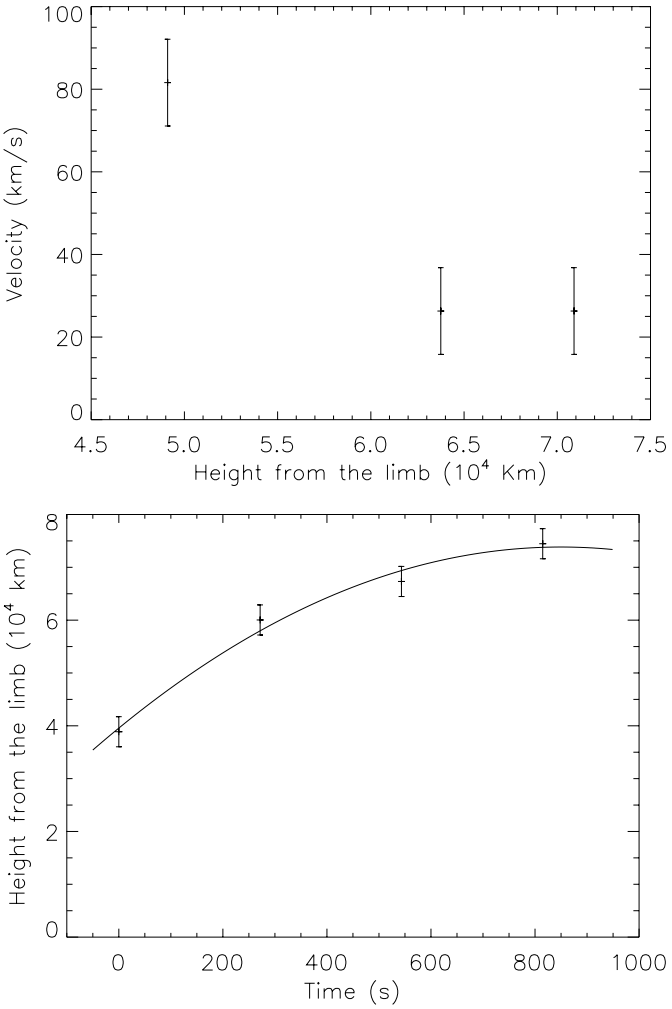

Fig. 9. Top: velocity v. height above the limb of the plasmoid expelled by the macrospicule. The values are taken from Table 1. Bottom: trajectory of the expelled plasmoid fitted over the estimated position.

6. Density and temperature

Following on from the discussion of Sect. 4, in which the ejection of a cloud of cool material from the chromosphere was proposed, the density and temperature characteristics are now considered. In the previous section it was shown that there was little evidence of bulk motion perpendicular to the radial direction. However, flows out from the limb in the radial direction were found. The speed appeared to decrease with time and tend towards about 26 km s^{-1}, reaching that value by about 60 000 km above the limb, that is, by the time of the exposure seen in Col. 5 of the raster.

The intensity profile in Col. 4 clearly shows the effect of the macrospicule structure, so these data were selected for further analysis, applying spectroscopic diagnostics to obtain temperature and density information. Implicit in

the analysis was the assumption that by this time the flow was sufficiently reduced to allow ionization equilibrium. It has already been shown in the previous section that the outflow velocity then was about 26 km s^{-1}.

It should be noted that the unsubtracted data were used because of the low signal in Col. 4 after the subtraction of the "background" data. In this way, a comparison between the "background" data and the "background plus macrospicule" data is possible, over a temperature range that goes from the cool emission of the macrospicule to that of the hot corona.

6.1. Density

Densities obtained using the line-ratio technique have been plotted in Fig. 10 as a function of distance, measured in arcsec along the slit direction. Results are shown for ions with peak emission at temperatures ranging from chromospheric to low coronal values: O IV ($T = 2{\times}10^5$ K), Mg VII ($T = 6.3 \times 10^5$ K), Mg VIII ($T = 7.9 \times 10^5$ K) and Si IX ($T = 1.3 \times 10^6$ K).

In the figure, the temperature of the emitting plasma increases from top to bottom. In spite of the quite large uncertainties, the density from O IV ($\log T = 5.3$) can be seen to increase with distance up to $-1020''$ by more than one order of magnitude, and then it starts decreasing.

The Mg VII ratio shows a different behaviour: first the density decreases, then increases up to about $-1030''$ and then decreases again. Also in this case the density changes by more than one order of magnitude.

The profiles derived from the Mg VIII and Si IX line ratios exhibit only small changes in density with distance, but still enough to show a slight decrease between $-1005''$ and $-1020''$ where it then rises towards higher values. Note that the rise visible in these last two profiles, is located two pixels ahead of the point where the density derived from O IV peaks, that is at $-1020''$.

From the trends shown in the figure, a possible qualitative interpretation can be drawn. The increase in O V intensity shown in Fig. 6, Col. 4 has been interpreted as the signature of an expelled cloud. If this is the case, the hot coronal material previously occupying the cloud volume will be displaced by cooler macrospicule plasma and will be pushed forward. This picture could justify the increased density seen from the oxygen ratio and the decrease in density from the other ratios, between $-1005''$ and $-1020''$ to $1030''$. The constant densities from the coronal lines, obtained below $-1005''$, together with the decrease in density from Mg VII and the increase seen in O IV at the same distances, may be an indication that at these distances the space is filling back with hot coronal plasma. Moreover, the step in density at $1030''$ seen in the hottest lines, may be interpreted as the hot material pushed ahead of the cool cloud.

It is important to remember that the density derived here is from emission integrated over the whole line of sight. This is the reason why major fluctuations in density

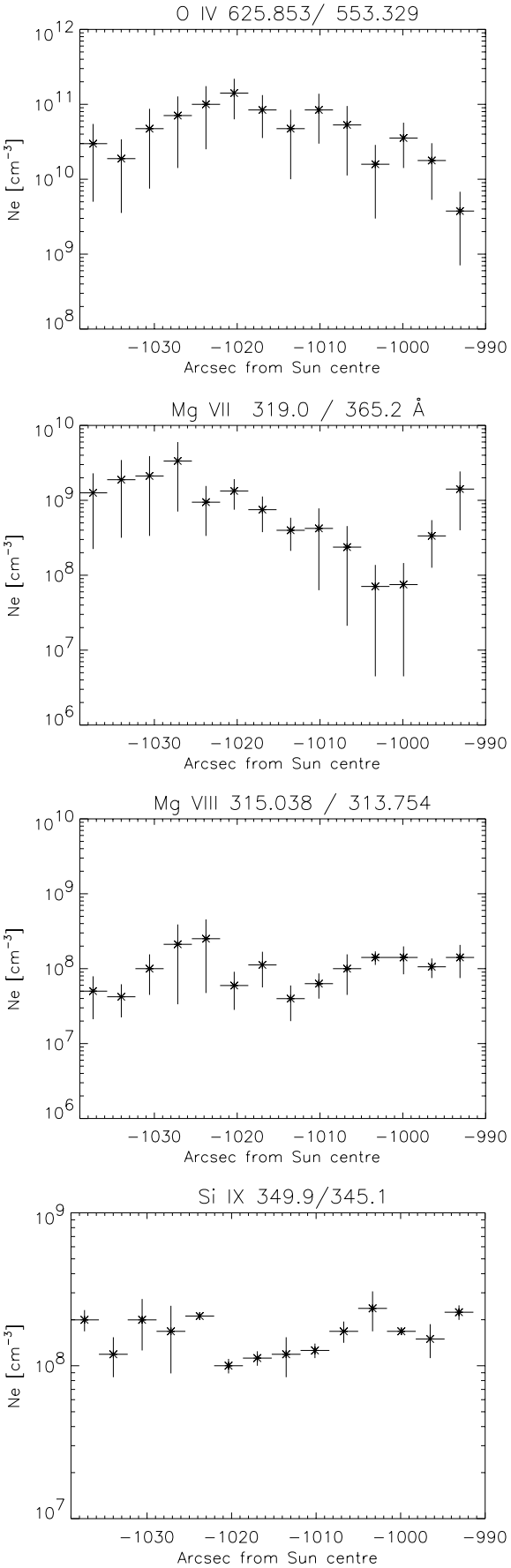

Fig. 10. Density along the solar distance in the Col. 4 for the macrospicule data. The error bars represent the probable error.

are seen using ratios of cooler lines. The observed O intensities are emitted predominantly by the feature: O IV and O V will not normally be seen in the off-limb hot corona. The observed Mg VIII and Si IX are, though, emitted in that region, so only a small contribution will originate from the volume occupied by the macrospicule.

An attempt to compare the density obtained here for the macrospicule, with that from the background was made. The Col. 4 background data was selected and a check of the spectra revealed that the only ratios usable for density diagnostics were the Mg VII and Si IX ones. The O IV ratio was too faint to be reliable.

The densities derived from the background are represented in Fig. 11 by asterisks. The densities from the macrospicule data (unsubtracted) were derived using the same line ratios; these are overplotted in the same figure using the diamond symbol. Looking at the magnesium ratio, for distances less than $-1010''$ the background density is higher than that in the macrospicule observation. Above that, the macrospicule material seems to become more dense. However, the silicon ratio shows that the densities are similar in the macrospicule and background. This provides further evidence in support of the interpretation given above.

6.2. Temperature

A comparison between the temperature behaviour of cool and hot plasma can be seen in Fig. 12. Here the temperature profiles derived from O V 629.7/O IV 554.5 Å, Ne VI 562.803/Ne V 572.33 Å and Mg X 624.9/Mg IX 368 Å ratios are shown. Each plot shows the values derived from the observations of the background (asterisk) and the macrospicule (diamond). In coronal holes, lines like oxygen and neon become faint not far from the limb, so that here the temperatures have been derived only for distances up to $-1040''$. The results show a small change with distance for both the macrospicule and the background. Clearly the plasma is not isothermal, because different ratios give different temperatures. Moreover, the Mg ratio indicates that there is no significant change in the temperature between the background and the macrospicule, except for a small region around $-1010''$. This is the location of the peak of the O V intensity attributed to the ejected material.

Fluctuations are visible in the background temperature from the O and Ne ratios, while the macrospicule seems to assume more stable values. In particular, the macrospicule oxygen temperature is higher than that of the background above $-1010''$. The temperature from the Ne, instead, is always lower in the macrospicule than in the background.

This temperature behaviour is consistent with the presence of the cold cloud at about $-1010''$, as will be discussed in the next section.

7. Discussion

The observed feature discussed in this paper has been classified as a macrospicule. The cool line visible in our

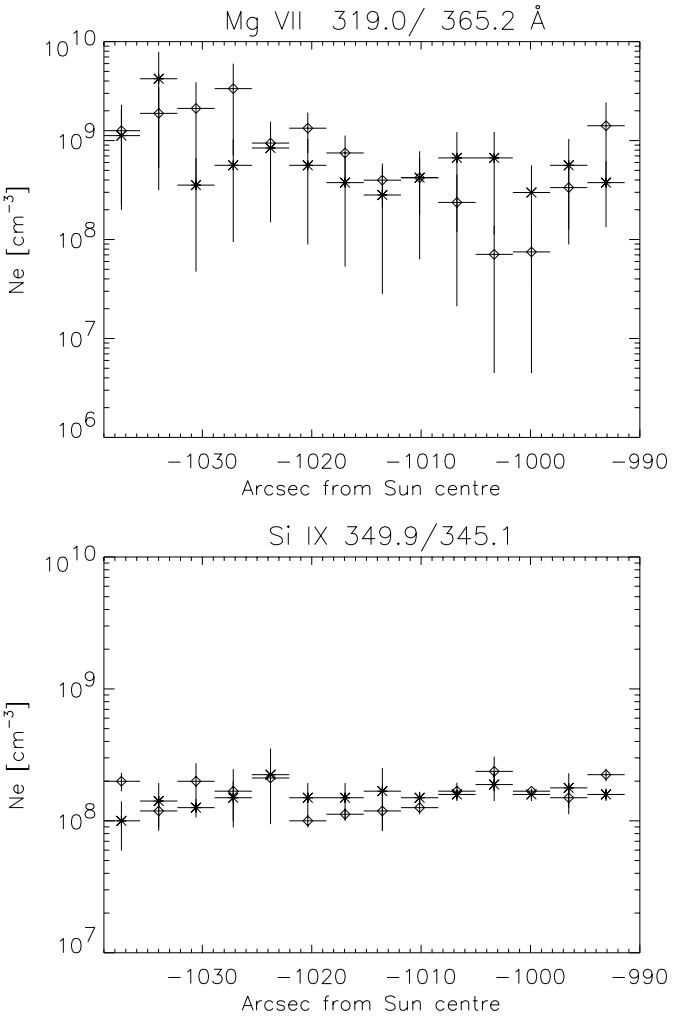

Fig. 11. Density from Mg VII 319.0/365.2 Å (top) Si IX (bottom): asterisks represent the observed background; diamonds the macrospicule observation (without background subtraction).

spectra, the He I ($\log T = 4.5$), showed it as a very bright feature, confirming that chromospheric material was ejected in the corona. The upper limit in temperature of the emitting macrospicule plasma was not easy to recognize. Clearly visible in transition region lines, the feature tended to disappear for temperatures above $\log T = 5.8$. However, a faint signature of the feature was present in the Mg IX 368.070 Å ($\log T = 6$, blended with a Mg VII $\log T = 5.8$) and seemed to become brighter in the Mg X lines ($\log T = 6$). The Mg X 624.941 Å line is blended with O IV at 625.126 and 625.853 Å so it is possible that the visibility of the feature at this wavelength is due to the cool oxygen line. The O IV 608.397 Å is far enough from the Mg X 609.793 Å to be resolved, but a strong O IV line is almost coincident with it at 609.827 Å.

The intensity profile was also checked for other lines emitted over a logarithmic temperature interval of about 5.9–6.1 (Fe X 345.7 Å, Ca X 557.5 Å, Si VIII 319.5 Å, Fe XII 364.5 Å). No indication of the macrospicule was visible. This supports the theory that the Mg X only appears

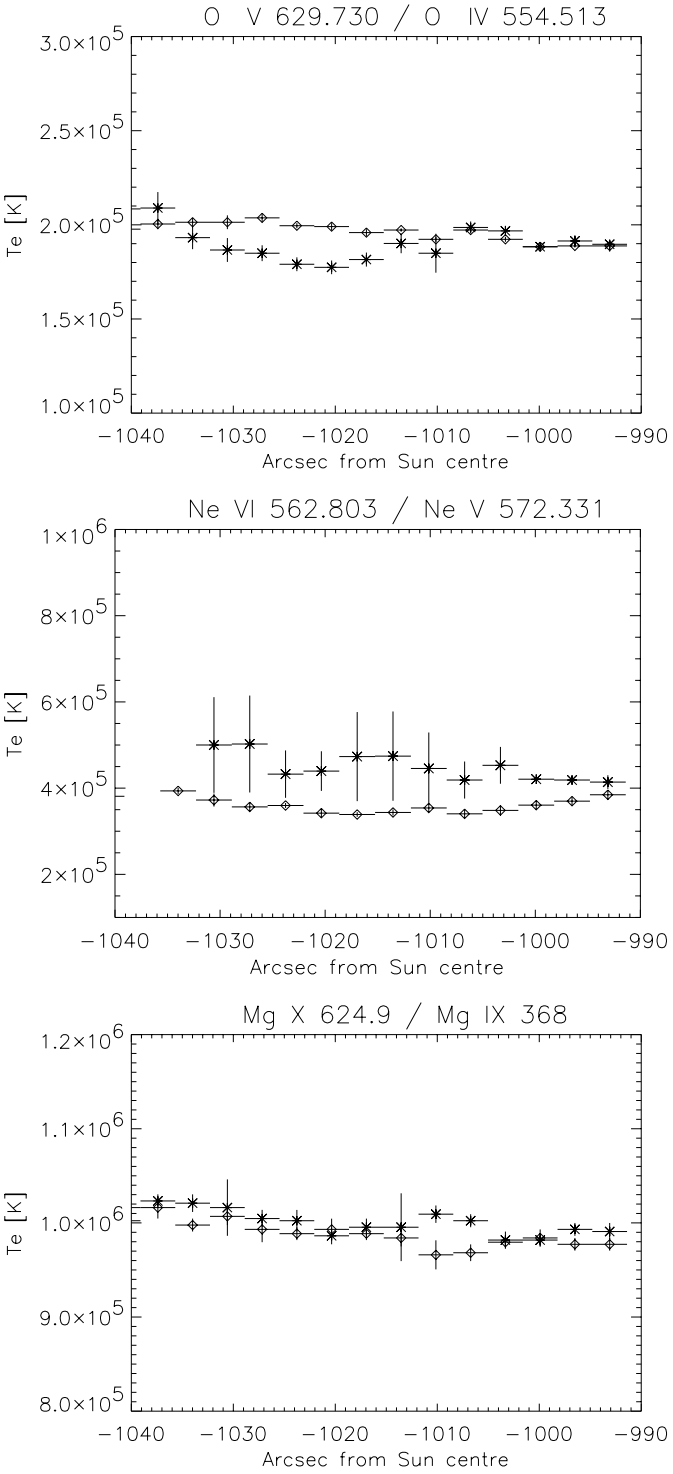

Fig. 12. Temperature derived from: the O V/IV (554.5); Ne VI 562.803/Ne V 572.331; Mg X 624.9/Mg IX 368; for the background (asterisk) and the exposure with the macrospicule (diamond).

to show the feature because it is influenced by the blend with O IV.

This question is still debated in the literature. Pike & Harrison (1997) and Banerjee et al. (2000), for example, claimed that their macrospicules were visible in the million degree temperature Mg IX line, while Wilhelm (2000) did not find any signature in the Mg X 624.41 Å (from SUMER, which has higher spectral resolution than CDS). Withbroe et al. (1976) saw a depletion in the same Mg X line, attributing this effect to the absorption of Lyman continuum at that wavelength. They found that the maximum absorption was located 20″ from the limb. That corresponds approximately to the lowest point of the observations presented here, and our Mg X line can be affected by blending with O IV in the region of the macrospicule, so we are unable to determine whether or not absorption was present.

In this work there is no significant indication that hot material is emitted by the macrospicule. The density and temperature results derived from different coronal line ratios in the macrospicule, showed that here there is no significant difference from the background values. The density values from the coronal Si IX line ratio are, moreover, in good agreement with the values derived by Fludra et al. (1999) above the quiet coronal hole.

However, density and temperature derived from ratios of lines emitted over transition region temperatures, show fluctuations that appear related to the presence of the feature already observed in the line intensities. Moreover, they are consistent with values derived from observations of macrospicules in radio wavelengths (Habbal & Gonzalez 1991), and in white light Hα (Loucif 1994).

The data from Col. 4 led to the interpretation that a cloud of cooler and denser material was expelled in the macrospicule. Comparing the peak of intensity in the O V and the density derived from the same element, the maximum distance reached by the core of the cloud is found to be 1020″ (46.2″, or 33 019 km from the limb), while the expansion front appeared to extend to about 75 000 km. This is comparable to results from previous studies which found expelled material reaching a distance of 39 000 km (Karovska & Habbal 1994) and 33 000 (Withbroe et al. 1976). However, lower values for the maximum altitude reached by these plasmoids were also recorded in H_α and H-Lyman lines (Delannee et al. 1998; Georgakilas et al. 1999). The authors justify these as a probable consequence of the hydrogen ionization that occurs as soon the chromospheric material is ejected into the hotter corona.

The outflow velocity estimated here does not appear to be as large as found for other short time-scale events like jets and turbulent events (i.e. Brueckner & Bartoe 1983; Wilhelm et al. 1998a; Ryutova & Tarbell 2000). The expansion velocities are comparable to the outflow velocity derived in the interplume regions (from O VI 1032/1037 ratio) of 67 km s^{-1} over the same distance by Patsourakos & Vial (2000), even though Wilhelm et al. (1998b) found a slightly lower velocity of about 40 km s^{-1} at 1.1 $R_\odot$ from Si VIII line widths in the interplume region. Our results from the study of the background, confirms that the macrospicule is not located in a plume environment where, instead, no measurable velocity has been detected (Wilhelm et al. 1998b). If the macrospicule and surrounding plasma have comparable velocities as the plasmoid

moves in the corona, not much compression of the plasma would be expected on the expansion front (about $-1030''$ in our case), although some variation in density and temperature was found here.

Only small line-of-sight components of velocity were found in these data. The maximum flow registered was about 17 km s^{-1} toward the red, while no blue-shifted component was detected. This could simply be interpreted as the effect of a small departure from the radial direction in the outward motion of the macrospicule plasma. The maximum velocity previously deduced from doppler-shifted EUV data, appeared to be located between $20''$ and $30''$ (Pike & Harrison 1997) and $30''$–$43''$ from the limb (Wilhelm 2000) with values higher than 100 km s^{-1}. These distances fall at or outside the lower limit covered by our data (where $30''$ above the limb is at about $-1004''$). On the other hand, Pike & Mason (1998) derived much lower values of a few tens of km s^{-1} at $40''$–$50''$ from the limb. It may be that as the material reaches a certain altitude the transverse velocity component reduces to zero, with our data set just too high to observe such transverse/rotational effects.

Studying the cloud trajectory, and applying a constant deceleration approximation, a value for the deceleration was found that is less than expected from the solar gravity. Previous studies attributed this to an inclination of the trajectory with respect to the line of sight (Karovska & Habbal 1994; Suematsu et al. 1995). These studies refer to spicules and macrospicules, and the characteristic inclination found ranges from 61° to 74° with respect to the radial direction. The value found here is close to that range. However, if this were the case, a Doppler shift effect on the lines would be expected. The line-shift study presented here, however, does not support this theory, because only velocities of the order of 17 km s^{-1} were found. Moreover, the data indicated that the deceleration was not constant. In particular, close to the limb it assumed a value close to the solar gravity, while at a larger distance it became almost zero. In conclusion, what seems more probable is that the feature was extending from the limb in an almost radial direction. Once the plasmoid was expelled, it decelerated under the influence of gravity until its speed was comparable to the ambient flow, with which it merged.

The important unresolved questions concern the mechanisms that generate these features and where they take place in the chromosphere. Wilhelm (2000) discussed the origin of spicules and macrospicules and, as other authors, suggested explosive events or a subclass of them (Wang 1998), due to reconnection in the chromospheric network boundary, as a possible origin for these features. In support of this, Karovska et al. (Karovska et al. 1994), using the image enhancement algorithm on Skylab images, resolved the fine structure at a macrospicule's base. They found a continuous interaction between the filamentary spicule-like substructure that evolved through reconnections. Unfortunately the present data lack any limb information and the macrospicule's base could not be studied.

To summarise, the signature of chromospheric material expelled from a coronal hole was found in intensity, density and temperature from chromospheric lines. These properties led to the classification of this event as a macrospicule. It appeared to be located in an interplume region of the south polar coronal hole. The data used here gave the unique opportunity to separate the emission of the feature from that of its background. This revealed the presence of a cool cloud released in the macrospicule, before its disappearance. The time evolution and outflow velocity of this cloud were studied, and the results showed that this short-lived feature ultimately expands into the corona with a steady velocity of the same order as that reported in interplume regions. As it moved outwards it displaced coronal material ahead of it, compressing this slightly. The flow was near-radial, with no rotational motion apparent at these altitudes.

Acknowledgements. The authors would like to acknowlege C. D. Pike for the helpful comments that improuved this paper. SP was supported by a University of Central Lancashire studentship and has used PPARC STARLINK computer facilities. SOHO is a mission of international cooperation of ESA and NASA. SP would like to thank the CHIANTI consortium for providing the atomic database. The authors are grateful to the EIT consortium for the provision of supporting images.

References

Banerjee, D., O'Shea, E., & Doyle, J. G. 2000, A&A, 355, 1152
Bohlin, J. D., Vogel, S. N., Purcell, J. D., et al. 1975, ApJ, 197, L133
Brueckner, G. E., & Bartoe, J. F. 1983, ApJ, 272, 329
Cook, J. W., Brueckner, G. E., Bartoe, J. F., & Socker, D. G. 1984, Adv. Space Res., 4, 59
Deforest, C. E., Hoeksema, J. T., Gurman, J. B., et al. 1997, Sol. Phys., 175, 393
Del Zanna, G. 1999, Ph.D. Thesis, Univ. of Central Lancashire
Del Zanna, G., & Bromage, B. J. I. 1999, in Ninth European Meeting on Solar Physics: Magnetic Fields and Solar Processes, Ninth Meeting of the Solar Physics Section of the Joint Astrophysics Division of the European Physical Society (EPS) and of the European Astronomical Society (EAS), Florence, Italy, 12–18 September, 1999, Proc. published in ESA SP Ser. (SP-448), ed. A. Wilson., E245
Del Zanna, G., Bromage, B. J. I., Landi, E., & Landini, M. 2001, A&A, 379, 708
Delannee, C., Koutchmy, S., Delaboudiniere, J., et al. 1998, in ESA SP-421: Solar Jets and Coronal Plumes, 129
Dere, K. P., Bartoe, J. F., Brueckner, G. E., Cook, J. W., & Socker, D. G. 1989, Sol. Phys., 119, 55
Fludra, A., del Zanna, G., Alexander, D., & Bromage, B. J. I. 1999, JGR, 104, 9709
Georgakilas, A. A., Koutchmy, S., & Alissandrakis, C. E. 1999, A&A, 341, 610
Habbal, S. R., & Gonzalez, R. D. 1991, ApJ, 376, L25
Harrison, R. A., Sawyer, E. C., Carter, M. K., et al. 1995, Sol. Phys., 162, 233
Haugan, S. V. H. 1997, CDS software note, 47
Karovska, M., Blundell, S. F., & Habbal, S. R. 1994, ApJ, 428, 854

Karovska, M., & Habbal, S. R. 1994, ApJ, 431, L59
Landi, E., Landini, M., Dere, K. P., Young, P. R., & Mason, H. E. 1999, A&AS, 135, 339
Loucif, M. L. 1994, A&A, 281, 95
Mariska, J. T. 1992, The solar transition region (Cambridge Astrophysics Series, New York: Cambridge University Press, c1992)
Mason, H. E., Young, P. R., Pike, C. D., et al. 1997, Sol. Phys., 170, 143
Mazzotta, P., Mazzitelli, G., Colafrancesco, S., & Vittorio, N. 1998, A&AS, 133, 403
Moore, R. L., Tang, F., Bohlin, J. D., & Golub, L. 1977, ApJ, 218, 286
Patsourakos, S., & Vial, J. 2000, A&A, 359, L1
Pike, C. D., & Harrison, R. A. 1997, Sol. Phys., 175, 457
Pike, C. D., & Mason, H. E. 1998, Sol. Phys., 182, 333
Ryutova, M. P., & Tarbell, T. D. 2000, ApJ, 541, L29
Suematsu, Y., Wang, H., & Zirin, H. 1995, ApJ, 450, 411
Wang, H. 1998, ApJ, 509, 461
Wilhelm, K. 2000, A&A, 360, 351
Wilhelm, K., Innes, E. E., Curdt, W., Kliem, B., & Brekke, P. 1998a, in ESA SP-421: Solar Jets and Coronal Plumes, 103
Wilhelm, K., Marsch, E., Dwivedi, B. N., et al. 1998b, ApJ, 500, 1023
Withbroe, G. L., Jaffe, D. T., Foukal, P. V., et al. 1976, ApJ, 203, 528
Young, P. R., Klimchuk, J. A., & Mason, H. E. 1999, A&A, 350, 286